ARTICLE IN PRESS

Computers and Mathematics with Applications xxx (xxxx) xxx

Contents lists available at ScienceDirect

Computers and Mathematics with Applications

journal homepage: www.elsevier.com/locate/camwa

A phase-field multirate scheme with stabilized iterative coupling for pressure driven fracture propagation in porous media

Mohamad Jammoul [a], Mary F. Wheeler [a], Thomas Wick [b,*]

[a] Center for Subsurface Modeling, Oden Institute for Computational Engineering and Sciences, The University of Texas at Austin, Austin, TX 78712, USA

[b] Leibniz Universität Hannover, Institut für Angewandte Mathematik, AG Wissenschaftliches Rechnen, Welfengarten 1, 30167 Hannover, Germany

ARTICLE INFO

Article history:
Available online xxxx

Keywords:
Phase-field fracture
Porous media
Multirate
Iterative coupling
Benchmarks

ABSTRACT

Phase-field methods have the potential to simulate large scale evolution of networks of fractures in porous media without the need to explicitly track interfaces. Practical field simulations require however that robust and efficient decoupling techniques can be applied for solving these complex systems. In this work, we focus on the mechanics-step that involves the coupling of elasticity and the phase-field variable. We develop a multirate scheme in which a coarser time grid is employed for the mechanics equation (i.e., the displacements) and a finer time grid is taken for the phase-field problem. The performance of this algorithm is demonstrated for two test cases.

© 2020 Elsevier Ltd. All rights reserved.

1. Introduction

According to the Wall Street Journal [1], thousands of shale wells drilled in the last five years are pumping less oil and gas than their owners forecast to investors, raising questions about the strength and profitability of the fracking boom that turned the U.S. into an oil superpower. Moreover, recent field observations indicate through field experimentations that current stimulation models fall short in predicting fracture geometries, proppant placement and transport and flowback and the effects of stress shadowing. These concerns provide opportunities for employing high fidelity advanced algorithms and mathematical models such as phase-field.

Phase-field models belong to the category of continuum approaches for fracture propagation utilizing a diffusive representation of cracks in place of actual discontinuities. The amount of crack regularization is controlled via a prescribed length scale, which constitutes an additional parameter of the model. These methods have potential to simulate large scale evolution of material microstructure and defect motion without the need to explicitly track interfaces. Francfort and Marigo [2] introduced a variational approach for Griffith's [3] quasi-static brittle fracture followed by numerics presented in [4]. This was later embedded into a thermodynamically consistent phase-field technique by Miehe et al. [5]. Using such a variational approach, discontinuities in the displacement field $\mathbf{u}$ across lower-dimensional crack surfaces are approximated by an auxiliary phase-field function φ, introducing a diffusive transition zone between the broken and the unbroken material. Important difficulties in phase-field fracture are the resolution of the length-scale parameter ε with respect to spatial discretization, the irreversibility of crack growth (yielding a variational inequality), and the nonlinear and linear solution of the overall system.

* Corresponding author.
E-mail address: thomas.wick@ifam.uni-hannover.de (T. Wick).

https://doi.org/10.1016/j.camwa.2020.11.009
0898-1221/© 2020 Elsevier Ltd. All rights reserved.

Please cite this article as: M. Jammoul, M.F. Wheeler and T. Wick, A phase-field multirate scheme with stabilized iterative coupling for pressure driven fracture propagation in porous media, Computers and Mathematics with Applications (2020), https://doi.org/10.1016/j.camwa.2020.11.009.

Phase-field models are attractive because crack nucleation, propagation, branching, and crack networks are included in the model. The variational principles allow to design numerical algorithms for which Galerkin finite elements can be employed. While there has been substantial work published on theoretical aspects of phase-field for porous media applications, few results have appeared on field problems [6–8]. This is due to lack of experimental data and accurate, efficient, and robust computational software.

The objective of this paper is to address the latter; namely improving the efficiency of phase-field fracture computations. We consider porous media in which flow and geomechanics interact, but the focus of this work is on the mechanics-step that involves the coupling of elasticity and the phase-field variable. Therein, the pressure from the flow problem is assumed to be given and acts like a right-hand-side term. Such a model was first proposed in [9]. A mathematical analysis of a decoupled version was conducted in [10] with corresponding numerical algorithms proposed in [11]. Recent reviews on pressurized fractures can be found in [12,13]. Technical difficulties arise inter alia through the crack irreversibility constraint, which is a variational inequality in time. In [11], an augmented Lagrangian penalization was applied yielding a robust numerical solution algorithm. Such a penalization includes a classical penalization parameter and an update function yielding a higher robustness with respect to ill-conditioning of the Jacobian matrix (i.e., the Hessian) due to the penalization process [14–16].

In the formulation used in this paper, the two subproblems, namely geomechanics and phase-field are decoupled. Subiterations are employed to achieve convergence of the coupled system. Sometimes, however, several hundreds of iterations are required. In the phase-field community, these decoupled iterations are known as alternating minimization [17,18]. Numerical analyses and various modifications are discussed in [17,19,20]. Recently, another decoupled scheme (known as the *L*-scheme; originally proposed in [21,22]) with (constant) stabilizing parameters was proposed and analyzed in [23]. Moreover, we add that in [23], the augmented Lagrangian penalization was employed yielding a combined iteration for both the crack irreversibility constraint and the stabilization. The latter helps to improve the efficiency, while ensuring the same accuracy as in undamped iterations.

This last work constitutes the basic algorithm as a starting point for the current paper. A further enhancement includes employing multirate schemes which have yielded significant computational speedups for solving flow and mechanics in porous media [24–26]. In the limit as $\varepsilon \to 0$, the phase-field equations have the character of diffusion–reaction equations that are well-known in chemical reactions. Generally, such equations require smaller time steps than Laplacian-type problems [27]. To this end, we develop a multirate scheme in which a coarser time grid is employed for the mechanics step (i.e., the displacement equation) and a finer time grid is taken for the phase-field problem.

The outline of this paper is as follows: In Section 2, we present the governing equations. Then, in Section 3, a multirate scheme is developed. In Section 4, two representative test cases are conducted. We summarize our findings in Section 5.

2. Equations

We introduce the notation and the underlying equations in this section. Let $B \subset \mathbb{R}^d$, $d = 2$ the total domain[1] wherein $\mathcal{C} \subset \mathbb{R}^{d-1}$ denotes the fracture and $\Omega \subset \mathbb{R}^d$ is the intact domain. The outer boundary is denoted by ∂B.

With the help of an elliptic (Ambrosio–Tortorelli) functional [28,29] defined in B, the one-dimensional fracture $\mathcal{C}$ is approximated by a domain such that

$$\frac{1}{2}\int_B \Big(\frac{1}{\varepsilon}(1-\varphi)^2 + \varepsilon|\nabla\varphi|^2\Big)\,dx \quad \to \quad \int_{\mathcal{C}} 1\,ds \quad \text{for } \varepsilon \to 0,$$

where $\varepsilon > 0$ is the phase-field regularization parameter. For variational fracture, such an approximation was first proposed in [4]. Here, the inner fracture boundary is denoted by $\partial\Omega_F$; see Fig. 1.

2.1. Phase-field fracture modeling

We now recapitulate the components for a phase-field model for mechanics and pressurized fractures in the porous media mechanics step. Thus, we follow the ideas from [30]. We are interested in two solution variables: the vector-valued displacements $\mathbf{u} : B \to \mathbb{R}^d$ and a smoothed scalar-valued indicator phase-field function $\varphi : B \to [0, 1]$. The latter satisfies $\varphi = 0$ in the fracture domain, $\varphi = 1$ in the intact region, and φ between 0 and 1 in the transition region. The half-width of this zone is $\varepsilon > 0$; see again Fig. 1. Fracture propagation is a loading-dependent process for which we introduce the loading interval $I := (0, T)$, where $T > 0$ is the final loading time and $t \in I$ the current time. We introduce the incremental steps:

$$0 =: t_0 < t_1 < \cdots < t_n < \cdots t_N := T.$$

The loading step size is denoted by $\Delta t := t_n - t_{n-1}$.

We introduce the crack irreversibility condition that must be enforced:

$$\partial_t \varphi \leq 0. \tag{1}$$

[1] In this work, we only consider $d = 2$, but our algorithms would also work for $d = 3$, which is left for future studies.

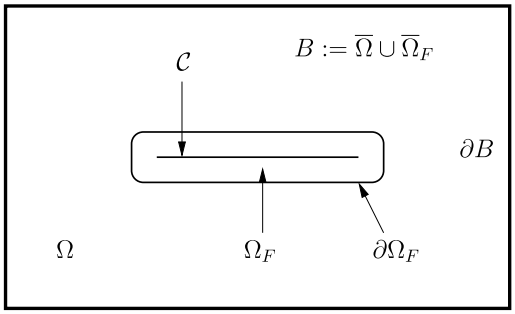

Fig. 1. Setup of the notation: the unbroken domain is denoted by Ω and $\mathcal{C}$ is the fracture. The latter one is approximated by the domain Ω_F. The half thickness of Ω_F is ε. The fracture boundary is $\partial\Omega_F$ and the outer boundary is ∂B.

This inequality constraint is treated using a difference quotient, resulting in

$$\varphi \leq \varphi^{n-1}.$$

Here, $\varphi^{n-1} := \varphi(t_{n-1})$ denotes the previous time step solution and $\varphi := \varphi(t_n)$ the current solution.

Next, we introduce function spaces in order to derive the variational formulations. To this end, let

$$V := H_0^1(B), \qquad W := H^1(B),$$

and for the inequality constraint we introduce the space

$$W_{in} := W_{in}(\varphi^{old}) := \{w \in H^1(B) |\, w \leq \varphi^{old} \leq 1 \text{ a.e. on } B\}.$$

Here, the L^2 scalar product is denoted by $\int_B \mathbf{u} \cdot \mathbf{v}\, dx =: (\mathbf{u}, \mathbf{v})$ for $\mathbf{u}, \mathbf{v} \in L^2(B)$.

To determine both unknowns $\mathbf{u}$ and φ, we start with an energy functional. For fractures in elastic solids, examples for such functionals go back to [2,4]. In the following, we extend such functionals for pressurized fractures. Therein, a time-dependent pressure $p := p(t) : B \times I \to \mathbb{R}$ becomes as a given term such as a right hand side. In [10][Section 2] and [30][Section 3.2], we used the divergence theorem to transform p from $\partial\Omega_F$ into the entire domain B. This procedure avoids knowledge of the exact fracture boundary location and is mathematically rigorous. As a consequence of the transformation, the pressure p is added as domain integral to the following energy functional. An example for updating the pressure is

$$p(t) = t\bar{p}, \quad \text{for given } \bar{p},$$

and $t \in I$ is the current time.

To this end, we obtain [10,30]:

Problem 2.1. Let $\varepsilon > 0$ and $\kappa > 0$ be phase-field regularization parameters and $\mathbf{n}$ the outward pointing normal vector. Let $p \in W^{1,\infty}(B)$ be given and let $\mathbf{u}^{n-1}$, φ^{n-1} be the previous time step solutions. Let $\mathbf{u}_D$ be an extension of Dirichlet data on a boundary part $\partial\Omega_D \subset \partial B$. For the loading increments $n = 1, 2, 3, \ldots, N$, we seek $\mathbf{u} := \mathbf{u}^n \in \{\mathbf{u}_D + V\}$ and $\varphi := \varphi^n \in W_{in}$ such that

$$\min_{\mathbf{u},\varphi} E_T(\mathbf{u}, \varphi)$$

with the pressurized energy functional:

$$\begin{aligned} E_T(\mathbf{u}, \varphi) = \frac{1}{2} \int_B \big((1-\kappa)\varphi^2 + \kappa\big)\sigma(\mathbf{u}) : e(\mathbf{u})\, dx \\ + \int_B \varphi^2 \big((1-\alpha) p \operatorname{div} \mathbf{u} + \nabla p \cdot \mathbf{u}\big)\, dx - \int_{\partial B} p\mathbf{n} \cdot \mathbf{u}\, ds \\ + \int_B G_c \big(\frac{1}{2\varepsilon}(1-\varphi)^2 + \frac{\varepsilon}{2}|\nabla\varphi|^2\big)\, dx. \end{aligned}$$

The critical energy release rate is denoted by $G_c > 0$ and the linear stress–strain relationship is given by:

$$\sigma := \sigma(\mathbf{u}) = 2\mu_s e(\mathbf{u}) + \lambda_s \operatorname{tr}(e(\mathbf{u}))I, \tag{2}$$

where $\operatorname{tr}(\cdot)$ is the trace operator, $\mu_s > 0$ and $\lambda_s > 0$ denote the Lamé coefficients, $e(u) = \frac{1}{2}(\nabla u + \nabla u^T)$ is the linearized strain tensor and I is the identity matrix. Biot's coefficient, $\alpha \in [0, 1]$, is chosen in this work as $\alpha = 0$.

Remark 2.1. When $\mathbf{u} = 0$ on ∂B then, the boundary integral vanishes. Furthermore, we assume constant pressures in this paper, i.e., $\nabla p = 0$. Then, the energy functional is modified as

$$\begin{aligned} E_T(\mathbf{u}, \varphi) = \frac{1}{2} \int_B \big((1-\kappa)\varphi^2 + \kappa\big)\sigma(\mathbf{u}) : e(\mathbf{u})\, dx \\ + \int_B \varphi^2 p \operatorname{div} \mathbf{u}\, dx \\ + \int_B G_c\big(\frac{1}{2\varepsilon}(1-\varphi)^2 + \frac{\varepsilon}{2}|\nabla\varphi|^2\big)\, dx. \end{aligned}$$

Non-constant pressures and $\alpha = 1$ work as well and were used for instance in [31,32]. The entire derivation of the previous energy functional and its mathematical analysis can be found in [10,30]. Based on these results, two types of algorithms were developed: monolithic schemes [33] and iterative coupling [11]. The latter is a computational starting point of this paper.

By taking the first variation of the previous energy functional from Remark 2.1, we obtain the following quasi-static coupled variational inequality system for pressurized phase-field fracture:

Problem 2.2. Let ε and κ be small regularization parameters. Let the pressure $p := p^n \in L^\infty(B)$ and $\mathbf{u}^{n-1}$, φ^{n-1} as the previous time step solutions be given. Find vector-valued displacements and a scalar-valued phase-field variable $\{\mathbf{u}, \varphi\} := \{\mathbf{u}^n, \varphi^n\} \in \{\mathbf{u}_D + V\} \times W$ such that

$$\Big(\big((1-\kappa)\varphi^2 + \kappa\big)\, \sigma(\mathbf{u}), e(\mathbf{w})\Big) + (\varphi^2 p, \operatorname{div} \mathbf{w}) = 0 \quad \forall \mathbf{w} \in V, \tag{3}$$

and

$$\begin{aligned} &(1-\kappa)(\varphi\, \sigma(\mathbf{u}) : e(\mathbf{u}), \psi - \varphi) + 2(\varphi\, p \operatorname{div} \mathbf{u}, \psi - \varphi) \\ &+ G_c\Big(-\frac{1}{\varepsilon}(1-\varphi, \psi-\varphi) + \varepsilon(\nabla\varphi, \nabla(\psi-\varphi))\Big) \geq 0 \quad \forall \psi \in W_{in} \cap L^\infty(B). \end{aligned} \tag{4}$$

From a mechanical point of view following [5,34], we furthermore distinguish fracture development under tension and compression, which is modeled by splitting the stress tensor σ by performing a spectral decomposition. To this end, we obtain

Problem 2.3. Let ε and κ be small regularization parameters. Let the pressure $p := p^n \in L^\infty(B)$ and $\mathbf{u}^{n-1}$, φ^{n-1} as the previous time step solutions be given. Find vector-valued displacements and a scalar-valued phase-field variable $\{\mathbf{u}, \varphi\} := \{\mathbf{u}^n, \varphi^n\} \in \{\mathbf{u}_D + V\} \times W$ such that

$$\begin{aligned} &\Big(\big((1-\kappa)\varphi^2 + \kappa\big)\, \sigma^+(\mathbf{u}), e(\mathbf{w})\Big) + (\sigma^-(\mathbf{u}), e(\mathbf{w})) \\ &\quad + (\varphi^2 p, \operatorname{div} \mathbf{w}) = 0 \quad \forall \mathbf{w} \in V, \end{aligned} \tag{5}$$

and

$$\begin{aligned} &(1-\kappa)(\varphi\, \sigma^+(\mathbf{u}) : e(\mathbf{u}), \psi - \varphi) + 2(\varphi\, p \operatorname{div} \mathbf{u}, \psi - \varphi) \\ &+ G_c\Big(-\frac{1}{\varepsilon}(1-\varphi, \psi-\varphi) + \varepsilon(\nabla\varphi, \nabla(\psi-\varphi))\Big) \geq 0 \quad \forall \psi \in W_{in} \cap L^\infty(B). \end{aligned} \tag{6}$$

In more detail, in Problem 2.3, the stress σ is split into tensile σ^+ and compressive parts σ^- as follows:

$$\begin{aligned} \sigma^+ &= 2\mu_s e^+ + \lambda_s [\operatorname{tr}(e)]_+ I, \\ \sigma^- &= 2\mu_s (e - e^+) + \lambda_s \big(\operatorname{tr}(e) - [\operatorname{tr}(e)]_+\big) I, \end{aligned}$$

and

$$e^+ = P \Lambda^+ P^T,$$

where $[\cdot]_+$ is the positive part of a function. Moreover, for $d = 2$, we have

$$\Lambda^+ := \Lambda^+(\mathbf{u}) := \begin{pmatrix} [\lambda_1(\mathbf{u})]_+ & 0 \\ 0 & [\lambda_2(\mathbf{u})]_+ \end{pmatrix},$$

where $\lambda_1(\mathbf{u})$ and $\lambda_2(\mathbf{u})$ are the eigenvalues of the strain tensor $e(\mathbf{u})$, and $v_1(\mathbf{u})$ and $v_2(\mathbf{u})$ the corresponding (normalized) eigenvectors. Finally, the matrix P is defined as $P := P(\mathbf{u}) := (v_1, v_2)$; namely, it consists of the column vectors v_i, $i = 1, 2$. Other laws can be found in [35] and [36].

2.2. An incremental formulation using augmented Lagrangian penalization

Starting from Problem 2.3, the phase-field variational inequality will be further relaxed in order to avoid solving the constraint system on a convex set. We follow [11] and apply an augmented Lagrangian formulation [14–16]. To this end, our strategy is as follows: we first discretize in time to obtain an incremental formulation. Applying the definition of the space W_{in}, the irreversibility constraint (1) is discretized with a backward difference quotient, where we now replace φ^{old} by φ^{n-1}:

$$\varphi \leq \varphi^{n-1}.$$

Here, $\varphi^{n-1} := \varphi(t^{n-1})$ denotes the previous time step solution and $\varphi := \varphi^n := \varphi(t^n)$ the current solution. If the constraint is violated, i.e., $\varphi > \varphi^{n-1}$, then an augmented Lagrangian formulation of the irreversibility constraint reads [11,33] and [13][Sec. 5.2.2.1]:

$$\Big[\Xi + \gamma(\varphi - \varphi^{n-1})\Big]_+$$

where $\Xi \in L^2$ is a Lagrange multiplier and $\gamma > 0$ a penalty parameter.

With these modifications, we obtain a system in which both variational statements are now of equality-type:

Problem 2.4. Let the regularization parameters $\kappa > 0$ and $\varepsilon > 0$ and the penalization parameter $\gamma > 0$ and the penalization function $\Xi \in L^2(B)$ be given. Let the pressure $p := p^n \in L^\infty(B)$ and $\mathbf{u}^{n-1}$, φ^{n-1} as the previous time step solutions be given. Find vector-valued displacements and a scalar-valued phase-field variable $\{\mathbf{u}, \varphi\} := \{\mathbf{u}^n, \varphi^n\} \in \{\mathbf{u}_D + V\} \times W$ such that

$$\Big(\big((1-\kappa)\varphi^2 + \kappa\big)\,\sigma^+(\mathbf{u}), e(\mathbf{w})\Big) + (\sigma^-(\mathbf{u}), e(\mathbf{w})) + (\varphi^2 p^n, \operatorname{div} \mathbf{w}) = 0 \quad \forall \mathbf{w} \in V, \tag{7}$$

and

$$\begin{aligned}&(1-\kappa)(\varphi\,\sigma^+(\mathbf{u}) : e(\mathbf{u}), \psi) + 2(\varphi\, p^n \operatorname{div} \mathbf{u}, \psi)\\ &+ G_c\Big(-\frac{1}{\varepsilon}(1-\varphi, \psi) + \varepsilon(\nabla\varphi, \nabla\psi)\Big)\\ &+ \Big([\Xi + \gamma(\varphi - \varphi^{n-1})]_+, \psi\Big) = 0 \quad \forall \psi \in W.\end{aligned} \tag{8}$$

Remark 2.2. We briefly notice that the penalization parameter $\gamma > 0$ is fixed and given. In practice, the function Ξ is updated iteratively as explained in Section 3. But of course, Ξ could also be approximated as an additional unknown without any sub-iterations; see for instance original monographs on the obstacle problem, e.g., [37]. For phase-field fracture such a formulation was recently introduced in [38].

2.3. Spatial discretization

The previous Eqs. (7) and (8) can be discretized in space using a classical Galerkin finite element method; see e.g., [39]. To this end, we introduce H^1 conforming discrete spaces $V_h \subset V$ and $W_h \subset W$ consisting of bilinear functions Q_1^c on quadrilaterals. The discretization parameter is denoted by h. For more details on the above system, we refer the reader to [11].

3. A phase-field fracture multirate scheme

In this section, a multirate scheme for a stabilized decoupled geomechanics-phase-field system is introduced. The stabilized decoupled method is known as L-scheme and was originally proposed in [22] for solving Richards' equation, which is a nonlinear elliptic–parabolic equation. The performance compared to other nonlinear methods, such as Newton's method, was investigated in [21]. The key idea of the L-scheme is to add stabilization terms, which link two subsequent solutions within an iteration. This idea was further applied to phase-field fracture in [23] in which the coupled system was solved in a decoupled fashion. Specifically, we introduced therein at a time point t_n, for the iteration index i, parameters $L_u > 0$ and $L_\varphi > 0$ and the following stabilization terms:

$$L_u\big(\mathbf{u}^{n,i} - \mathbf{u}^{n,i-1}, \mathbf{w}\big),$$
$$L_\varphi\big(\varphi^{n,i} - \varphi^{n,i-1}, \psi\big).$$

In [23] (specifically for the system (7) and (8)) the stabilization parameters L_u and L_φ where chosen as constants in order to establish a rigorous numerical analysis.

This approach is the starting point for our multirate formulation, which we shall describe in detail in this section. Therein, coarser time steps are chosen for the geomechanics equation, while smaller sub-time steps are adopted for the phase-field subsystem.

3.1. L-scheme for stabilization

The L-scheme is adopted to stabilize each of the mechanics and phase-field sub-problems. Parameters L_u and L_φ are introduced into Eqs. (7) and (8) to penalize the incremental change for displacement and degradation (phase-field) respectively. For constant stabilization parameters, a rigorous numerical analysis was established in [23]. The stabilized iterative scheme reads as follows [40]:

Problem 3.1. At time t_n, let $p := p^n \in L^\infty(B)$ and the previous time step solutions $\mathbf{u}^{n-1}$, φ^{n-1} be given. Set the initial iterates as $\mathbf{u}^{n,0} := \mathbf{u}^{n-1}$ and $\varphi^{n,0} := \varphi^{n-1}$ and $\Xi^0 = 0$. Iterating over $i = 1, 2, 3, \ldots$, given $\varphi^{n,i-1} \in W$, find first vector-valued displacements $\mathbf{u}^{n,i} \in \{\mathbf{u}_D + V\}$ such that

$$\begin{aligned} a_u\big(\mathbf{u}^{n,i}, \mathbf{w}\big) = L_u\big(\mathbf{u}^{n,i} - \mathbf{u}^{n,i-1}, \mathbf{w}\big) + \Big(\big((1-\kappa)(\varphi^{n,i-1})^2 + \kappa\big)\, \sigma^+(\mathbf{u}^{n,i}), e(\mathbf{w})\Big) \\ + (\sigma^-(\mathbf{u}^{n,i}), e(\mathbf{w})) + ((\varphi^{n,i-1})^2 p, \operatorname{div} \mathbf{w}) = 0 \quad \forall \mathbf{w} \in V, \end{aligned} \tag{9}$$

and now given $\mathbf{u}^{n,i}$, find a scalar-valued phase-field $\varphi^{n,i} \in W$ such that

$$\begin{aligned} a_\varphi\big(\varphi^{n,i}, \psi\big) = L_\varphi\big(\varphi^{n,i} - \varphi^{n,i-1}, \psi\big) + (1-\kappa)\Big(\varphi^{n,i}\, \sigma^+(\mathbf{u}^{n,i}) : e(\mathbf{u}^{n,i}), \psi\Big) \\ + 2(\varphi^{n,i}\, p \operatorname{div} \mathbf{u}^{n,i}, \psi) + G_c\Big(-\frac{1}{\varepsilon}(1-\varphi^{n,i}, \psi) + \varepsilon(\nabla\varphi^{n,i}, \nabla\psi)\Big) \\ + \Big([\Xi^i + \gamma(\varphi^{n,i} - \varphi^{n-1})]_+, \psi\Big) = 0 \quad \forall \psi \in W. \end{aligned} \tag{10}$$

In the previous problem statement, Ξ^i is updated as follows [13][p. 166]:

Algorithm 1 Update formula for the augmented Lagrangian penalization

At time step index n and iteration index i:

1. Solve (9)
2. Given Ξ^i, solve (10)
3. Update $\Xi^{i+1} := [\Xi^i + \gamma(\varphi^{n,i} - \varphi^{n-1})]_+$
4. Increment $i \to i+1$

It is well known that the optimal values for the stabilization parameters L_u and L_φ change during the solution procedure and in principle the stabilization parameters $L_u > 0$ and $L_\varphi > 0$ can be updated independently with different values. In [23] and [40], we found that $L := L_u = L_\varphi$ yields satisfactory results. For this reason, we simply go with this choice in the current work as well. We adopt constant values for the stabilization parameters L_u and L_φ to be able to study the performance of the multirate scheme. Constant values allow for a more rigorous analysis and computational evaluation as shown in [23]. Consequently, in the rest of this work, we assume $L_u = L_\varphi = 10^{-6}$ which is a heuristic trade-off between using a large value of L_i and not having any stabilization at all.

We also notice that an overall improvement of the computational cost can be achieved with a dynamic update of $L := L_u = L_\varphi$ during the subiterations. Detailed discussions can be found in [13,40]. To apply these dynamic adjustments along with the multirate scheme may be future work.

3.2. Multirate formulation

The mechanics equation (9) in the decoupled system is of an elliptic type and thus a coarse time step can be used for its solution. The phase-field equation (10) is similar to a reaction–diffusion partial differential equation requiring finer time steps. The proposed multirate scheme uses a different time step for each of the physical processes with the mechanics time step being a multiplier of the phase-field time step. The choice of the q-factor, the ratio of the mechanics time step to that of the phase-field time step, is set a priori; however one possible extension is to use an adaptive ratio based on a posteriori error estimates.

Iterative coupling is introduced at the time points where both equations are being solved. The mechanics equation is solved first with a coarse time step and then multiple phase-field sub-problems, with finer time steps, are solved consecutively. This procedure is repeated until the system of equations converges within a certain tolerance at the coarse time step. Fig. 2 shows an example of the different rates (time meshes) that the decoupled system can be solved.

The multirate formulation of Eqs. (9) and (10) yields our main result of this work:

Proposition 3.1. *At time t_n, let $p := p^n \in L^\infty(B)$ and the previous time step solutions $\mathbf{u}^{n-1}$, φ^{n-1} be given. Let the subiteration index for the smaller time step size be $k = 1, 2, \ldots, q$. Set the initial iterates as $\mathbf{u}^{n,0} := \mathbf{u}^{n-1}$ and $\varphi^{n,0} := \varphi^{n-1}$ and $\varphi_0^{n,i} := \varphi_{k=q}^{n,i-1}$ and $\Xi^0 = 0$. Iterating over $i = 1, 2, 3, \ldots$, yields*

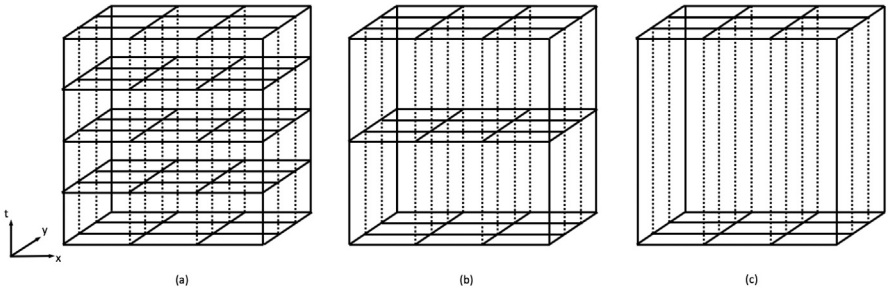

Fig. 2. Solving the phase-field and mechanics equations with three different q-factor values. The phase-field equation is solved on mesh (a) with fine time refinement. The mechanics equation can be solved with same time step (q = 1) (a), 2x time step (q = 2) (b), or 4x time step (q = 4) (c).

- *Step 1: Given* $(\mathbf{u}^{n,i-1}, \varphi_{k=q}^{n,i-1})$ *find* $\mathbf{u}^{n,i} \in \{\mathbf{u}_D + V\}$ *such that:*

$$\begin{aligned} a_u\big(\mathbf{u}^{n,i}, \mathbf{w}\big) &:= L_u\big(\mathbf{u}^{n,i} - \mathbf{u}^{n,i-1}, \mathbf{w}\big) + \Big(\big((1-\kappa)(\varphi^{n,i-1})^2 + \kappa\big)\, \sigma^+(\mathbf{u}^{n,i}), e(\mathbf{w})\Big) \\ &+ (\sigma^-(\mathbf{u}^{n,i}), e(\mathbf{w})) + ((\varphi^{n,i-1})^2 p, div\ \mathbf{w}) = 0 \quad \forall \mathbf{w} \in V. \end{aligned} \tag{11}$$

- *Step 2: Given* $(\varphi_{k-1}^{n,i}, \mathbf{u}^{n,i})$ *find* $\varphi_k^{n,i} \in W$ *for* $k = 1, 2, \ldots, q$ *such that:*

$$\begin{aligned} a_\varphi\big(\varphi_k^{n,i}, \psi\big) &= L_\varphi\big(\varphi_k^{n,i} - \varphi_{k-1}^{n,i}, \psi\big) + (1-\kappa)(\varphi_k^{n,i}\, \sigma^+(\mathbf{u}^{n,i}) : e(\mathbf{u}^{n,i}), \psi) \\ &+ 2(\varphi_k^{n,i}\, p\ div\ \mathbf{u}^{n,i}, \psi) + G_c\Big(-\frac{1}{\varepsilon}(1-\varphi_k^{n,i}, \psi) + \varepsilon(\nabla\varphi_k^{n,i}, \nabla\psi)\Big) \\ &+ \Big([\Xi^i + \gamma(\varphi_k^{n,i} - \varphi^{n-1})]_+, \psi\Big) = 0 \quad \forall \psi \in W. \end{aligned} \tag{12}$$

- *Step 3: Update* $\Xi^{i+1} := [\Xi^i + \gamma(\varphi_{k=q}^{n,i} - \varphi^{n-1})]_+$.

The pressure p^n *is updated after each marco time step when incrementing from* $n-1 \mapsto n$. *A detailed solution algorithm is described in the next section.*

3.3. Solution algorithm

The solution algorithm is based on the iterative coupling of Eqs. (11) and (12) until the residual of each equation is less than a pre-set tolerance. The residual is checked at the common time points only (coarse time steps). If convergence is not achieved, one mechanics step is executed followed by multiple phase-field solves. Algorithm 2 summarizes the solution procedure.

Algorithm 2 Multirate formulation of phase-field in the mechanics-step of porous media

At loading step t^n (or pressure p^n).
  repeat for $i = 1, 2, 3, \ldots$
    Solve the mechanics step (Eq. (11))
    while $k \leq q$ **do**
      Solve the phase-field step (Eq. (12))
      $k = k + 1$
    end while
    Update $\Xi^{i+1} := [\Xi^i + \gamma(\varphi_{k=q}^{n,i} - \varphi^{n-1})]_+$
    $i = i + 1$
  until $max\ (\|a_u\big(\mathbf{u}^{n,i}, \mathbf{w}\big)\|_{l^2}, \|a_\varphi\big(\varphi_{k=q}^{n,i}, \psi\big)\|_{l^2}) \leq TOL$
  Set $\{\mathbf{u}^n, \varphi^n\} := \{\mathbf{u}^{n,i}, \varphi_{k=q}^{n,i}\}$
  $t^{n+1} = t^n + \Delta t$

Remark 3.1. Inside Algorithm 2, both subproblems are nonlinear because of the nonlinear constitutive materials laws in Eq. (11) and the augmented Lagrangian regularization in Eq. (12). Consequently, Newton-type solvers are applied to each sub-system. Details on Newton's method for phase-field fracture can be found for instance in [13,33,41,42]. Inside Newton's method, the linear equation systems are solved with the direct solver UMFPACK [43].

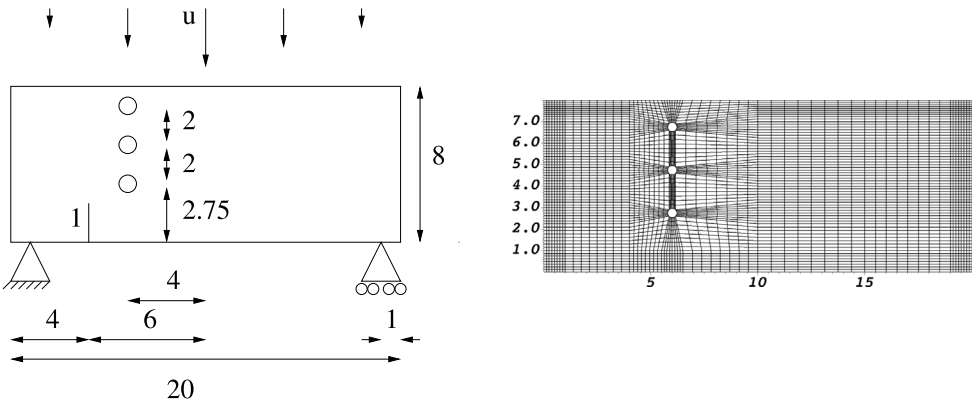

Fig. 3. Example 1: Asymmetric notched three point bending test. The geometry, loading and boundary conditions are taken from [44]. The three holes have each a diameter of 0.5. All units are in *mm*. At right, the initial mesh is displayed with 3904 cell elements.

4. Numerical tests

We conduct two numerical tests: fracture propagation with rate-dependent boundary conditions and pressurized crack growth. We focus on studying the performance of the multirate scheme in terms of accuracy and computational efficiency. For each of the two examples, we first present the numerical solution of a reference test case, and then we consider multiple test cases with coarser time steps. The coarse time steps considered are factors of the reference case time step (Δt_{ref}). For each test case, we compare the solutions of the multirate scheme with that of the single-rate scheme. The error in the solution of the phase field variable is reported with respect to that of the reference case.

4.1. Asymmetric three-point bending

We address an asymmetric three point bending test, which was previously considered by others as well [5,20,23,36] and was originally inspired by numerical and experimental setups from [44].

4.1.1. Configuration

The configuration including geometry data (in *mm*) is shown Fig. 3. The specimen is deformed using a smoothly-in-space displacement on the entire top boundary Γ_{top}:

$$\mathbf{u}(t, x, y = 8) = -10.0 * t * \exp(-(x - 10.0)^2/100).$$

For the reference case, $t = 6.25 * 10^{-5} \sum_i^{288} i$ denotes the loading parameter for which we compute a total of 288 loading steps.

The choice to prescribe $\mathbf{u}$ as boundary condition over the entire top boundary Γ_{top} was made in order to avoid a mathematically ill-posed setting by using a 'true' point displacement. As explained in [20], in the most left and right parts of the domain, the phase-field variable is fixed to $\varphi = 1$ in order to avoid artificially-induced cracks to due the loading and the boundary conditions. We briefly mention that the pressure is $p = 0$ in this test case.

The initial mesh (Fig. 3, right) is refined uniformly twice (each element is divided into 16 cells) yielding 62,464 mesh elements with minimal mesh size parameter $h = 0.033$[mm], and 63,198 degrees of freedom for the phase field variable (φ), and 126,396 degrees of freedom for displacement ($\mathbf{u}$).

4.1.2. Parameters

As material parameters, we use $\mu_s = 8\,\text{kN/mm}^2$, $\lambda_s = 12\,\text{kN/mm}^2$, and $G_c = 1 \times 10^{-3}\,\text{kN/mm}$. Furthermore, we set $\kappa = 10^{-10}h$ [mm] and $\varepsilon = 2h$. The penalization parameter is chosen as $\gamma = 10^{-4}$ and the initial Lagrange multiplier is set to $\Xi^0 = 0$. The tolerance of convergence for the augmented Lagrangian method is $TOL = 10^{-4}$.

4.1.3. Results

The propagation of the fracture for the reference case is displayed in Fig. 4. Fig. 4a–d show the evolution of the phase-field variable at four time instants. Numerical simulations were conducted for this example taking four different coarse time steps: $\Delta t = 12.5 \times 10^{-5}$ s ($2\Delta t_{ref}$), $\Delta t = 25 \times 10^{-5}$ s ($4\Delta t_{ref}$), $\Delta t = 50 \times 10^{-5}$ s ($8\Delta t_{ref}$), and $\Delta t = 74 \times 10^{-5}$ s ($12\Delta t_{ref}$). Each of these cases were simulated using a single-rate scheme and a multirate scheme. For the multirate scheme, the q-factors used were: $q = 2$, $q = 4$, $q = 8$, and $q = 12$ respectively. The end of simulations results of the single-rate scheme simulations are presented in Fig. 5. The results using the multirate scheme are in shown in Fig. 6.

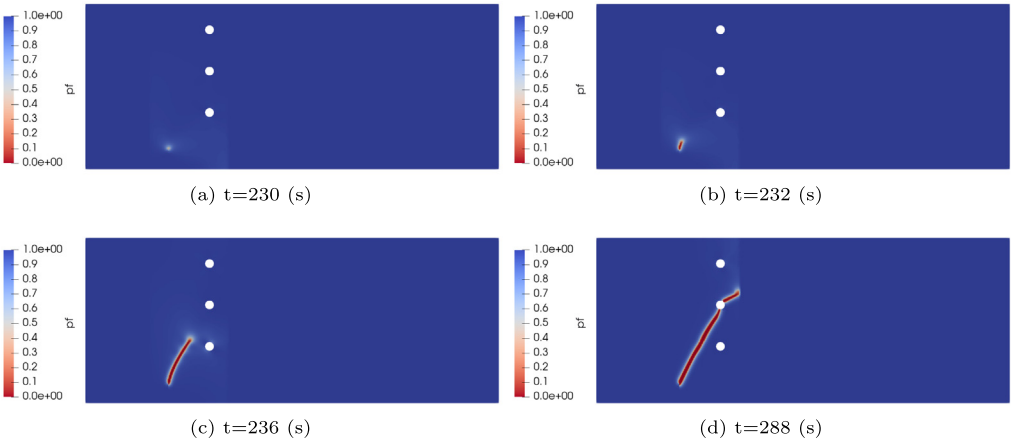

(a) t=230 (s) (b) t=232 (s)

(c) t=236 (s) (d) t=288 (s)

Fig. 4. Example 1: Fracture propagation with time.

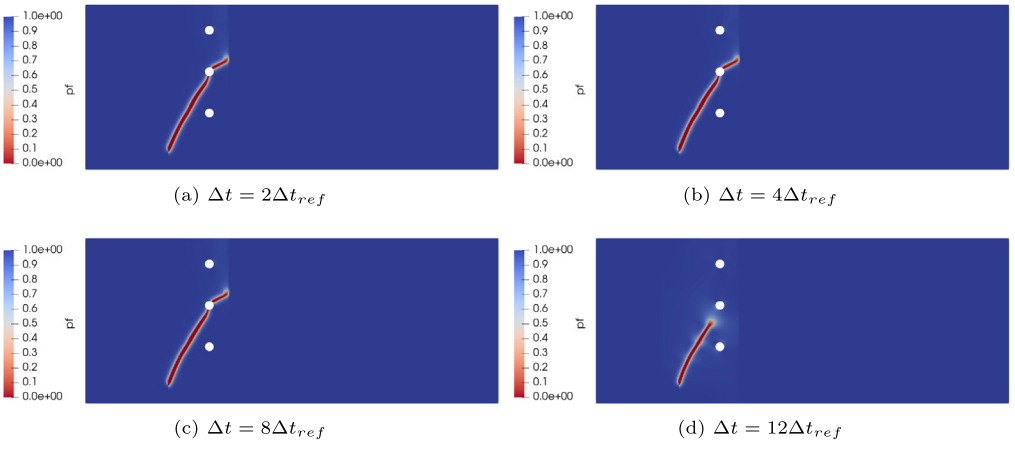

(a) $\Delta t = 2\Delta t_{ref}$ (b) $\Delta t = 4\Delta t_{ref}$

(c) $\Delta t = 8\Delta t_{ref}$ (d) $\Delta t = 12\Delta t_{ref}$

Fig. 5. Example 1: Comparison of fracture path at the end of simulations using single-rate scheme with four different time steps (Δt).

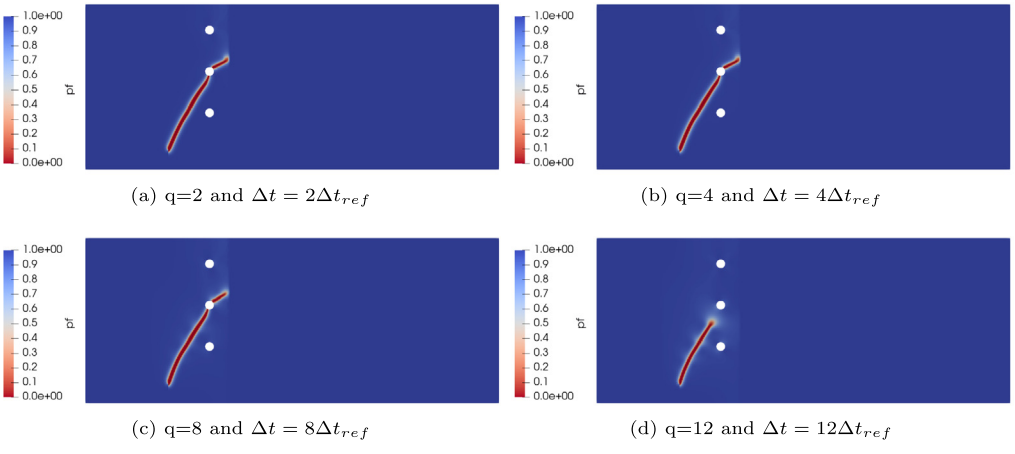

(a) q=2 and $\Delta t = 2\Delta t_{ref}$ (b) q=4 and $\Delta t = 4\Delta t_{ref}$

(c) q=8 and $\Delta t = 8\Delta t_{ref}$ (d) q=12 and $\Delta t = 12\Delta t_{ref}$

Fig. 6. Example 1: Comparison of fracture path at the end of simulations for four multirate factors.

As expected, using a coarse time step leads to less accurate numerical solutions as it is evident in Fig. 5d, where the fracture failed to propagate fully as compared to Fig. 4d. Even with using a multirate scheme Fig. 6d, the fracture path at the end of simulations failed to trace that of the reference test case when using a large time step ($\Delta t = 12\Delta t_{ref}$).

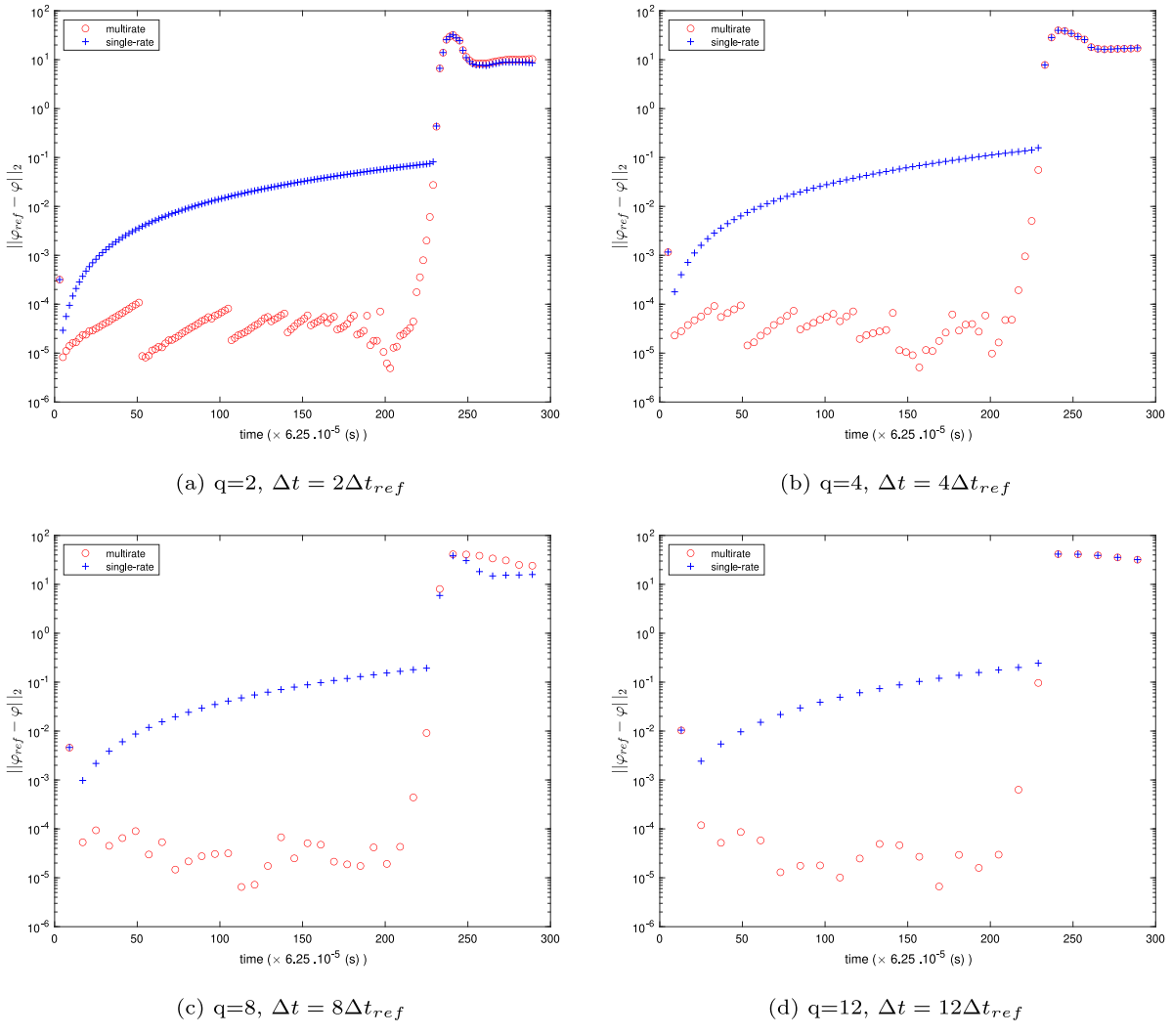

(a) q=2, $\Delta t = 2\Delta t_{ref}$ (b) q=4, $\Delta t = 4\Delta t_{ref}$

(c) q=8, $\Delta t = 8\Delta t_{ref}$ (d) q=12, $\Delta t = 12\Delta t_{ref}$

Fig. 7. Example 1: The error of different coarse time steps (Δt) is plotted over the simulation time for multirate and single-rate formulations.

In Fig. 7, we quantify the error for taking a coarse time step and compare the gained accuracy using the multirate scheme. The sum of the L_2-norm of the error in the phase-field variable over all the grid cells is plotted for each test case. The results show that the multirate scheme leads to a reduction in the error by $2-3$ orders of magnitude for the first 230 time steps. Beyond that point, the error of using a coarse time step increases significantly that the multirate scheme has little effect on the accuracy. This observation is reasonable as boundary conditions or largely broken materials influence clearly the numerical solution. Moreover, once the fracture reaches the hole, the solutions heavily differ as discussed in the literature [5,20,23,36].

From a computational efficiency perspective, the multirate iterations do not incur a high computational cost thus leading to total simulation time comparable to that of using a coarse time step (Fig. 8a). Taking efficiency and accuracy and into consideration, using a multirate scheme resulted in significant speedup (Fig. 8a) and relatively small error values (Figs. 8b) compared to the reference fine time step solution. However, we also notice that the coarse time step size should not be taken too coarse.

4.2. A propagating pressurized fracture

In this second test, we consider a pressurized propagating fracture. The pressure p is given as a known time-dependent function. To this end, we only solve the porous media mechanics-step, namely geomechanics with a given, known, pressure. This procedure allows a clear study on the performance of the proposed multirate scheme. The configurations of the proposed test cases are taken from [11,33].

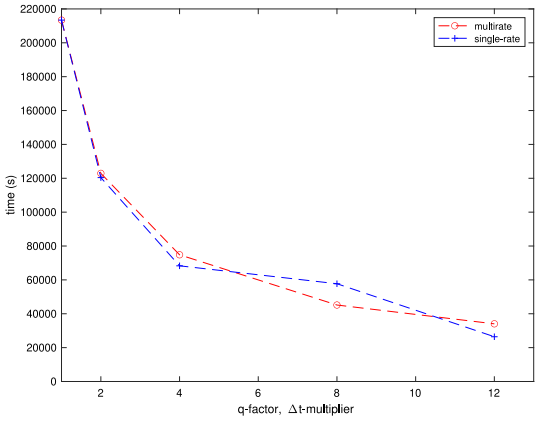

(a) Total simulation time for the single-rate and multirate schemes. Points are connected for visualization preferences.

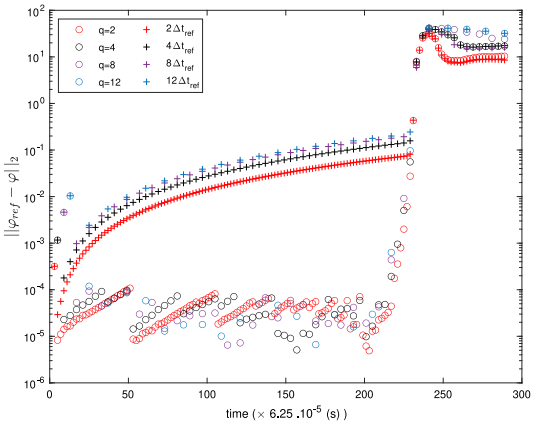

(b) Error in the phase-field variable over time

Fig. 8. Example 1: Comparison of speedup and accuracy of the multirate scheme. On the left, the total simulation time for the multirate scheme is compared to the single-rate formulation with a coarse time step. On the right, a comparison of the error in the phase-field solution for different q-factors is shown.

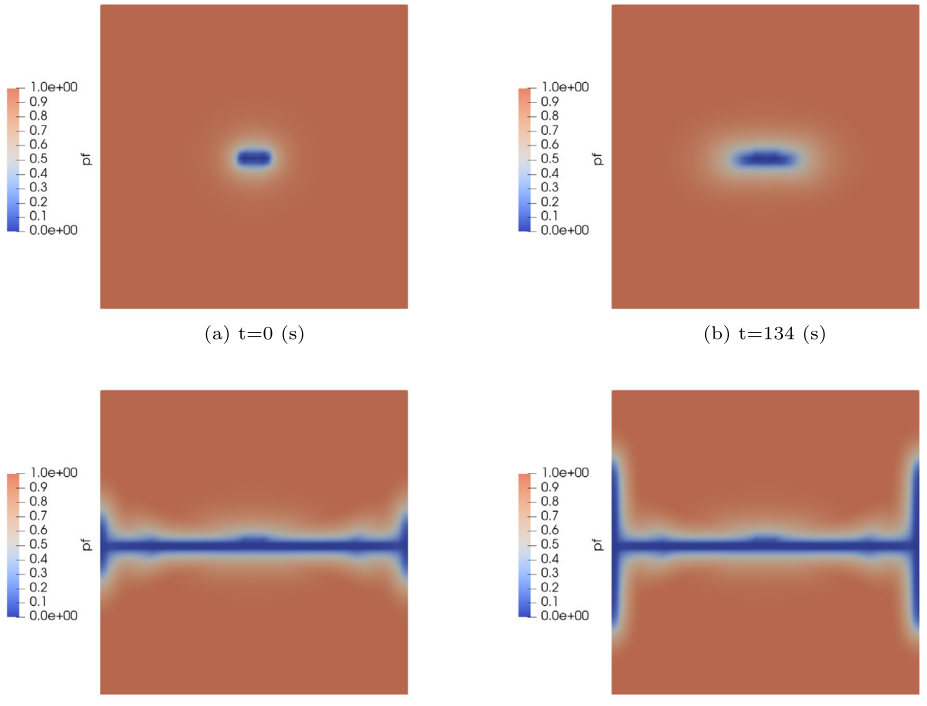

(a) t=0 (s) (b) t=134 (s)

(c) t=136 (s) (d) t=144 (s)

Fig. 9. Example 2: Fracture propagation with time.

4.2.1. Configuration

We deal with the following geometric data: $\Omega = (0\ m, 4\ m)^2$ and a (prescribed) initial crack with half length $l_0 = 0.2m$ on $\Omega_F = (1.8 - h, 2.2 + h) \times (2 - h, 2 + h) \subset \Omega$. This initial crack is given with the help of the phase-field function φ. We set at $t = 0$:

$$\varphi = 0 \quad \text{in } \Omega_F, \quad \text{and} \quad \varphi = 1 \quad \text{in } B \setminus \Omega_F. \tag{13}$$

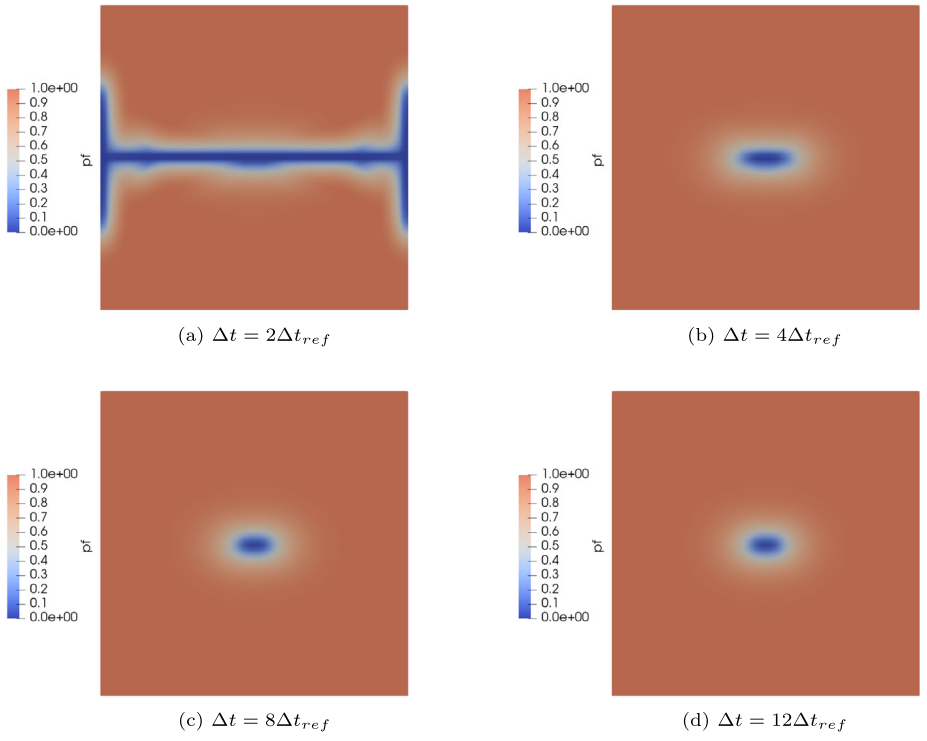

(a) $\Delta t = 2\Delta t_{ref}$ (b) $\Delta t = 4\Delta t_{ref}$

(c) $\Delta t = 8\Delta t_{ref}$ (d) $\Delta t = 12\Delta t_{ref}$

Fig. 10. Example 2: Comparison of the fracture path at the end of the simulations using a single-rate scheme with four different time steps (Δt).

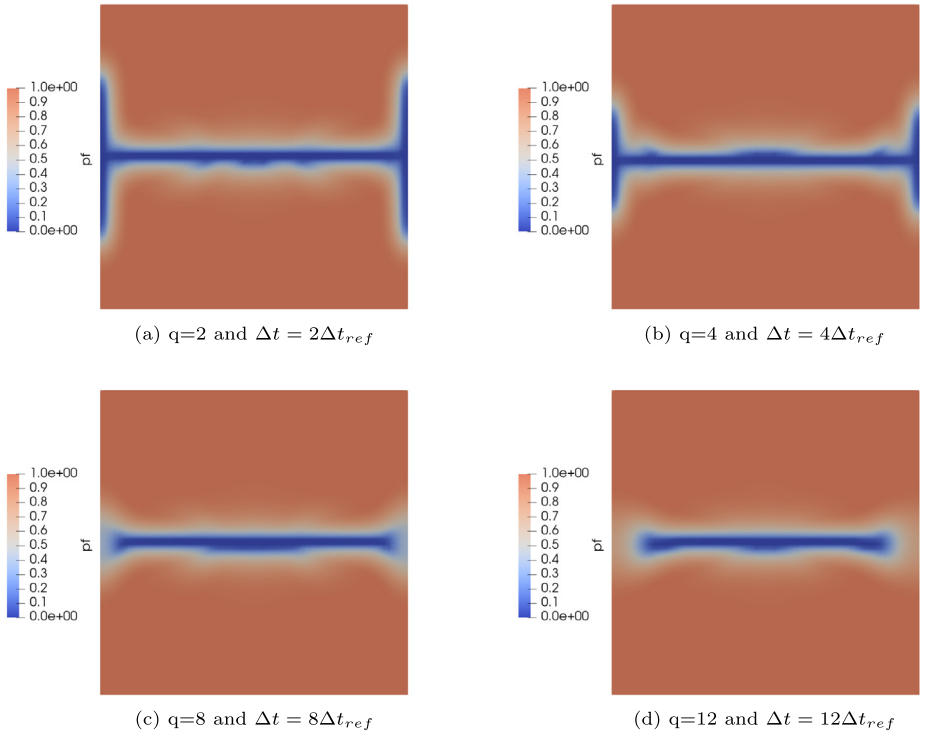

(a) q=2 and $\Delta t = 2\Delta t_{ref}$ (b) q=4 and $\Delta t = 4\Delta t_{ref}$

(c) q=8 and $\Delta t = 8\Delta t_{ref}$ (d) q=12 and $\Delta t = 12\Delta t_{ref}$

Fig. 11. Example 2: Comparison of the fracture path in terms of the phase-field variable φ at the end of simulations for four multirate factors.

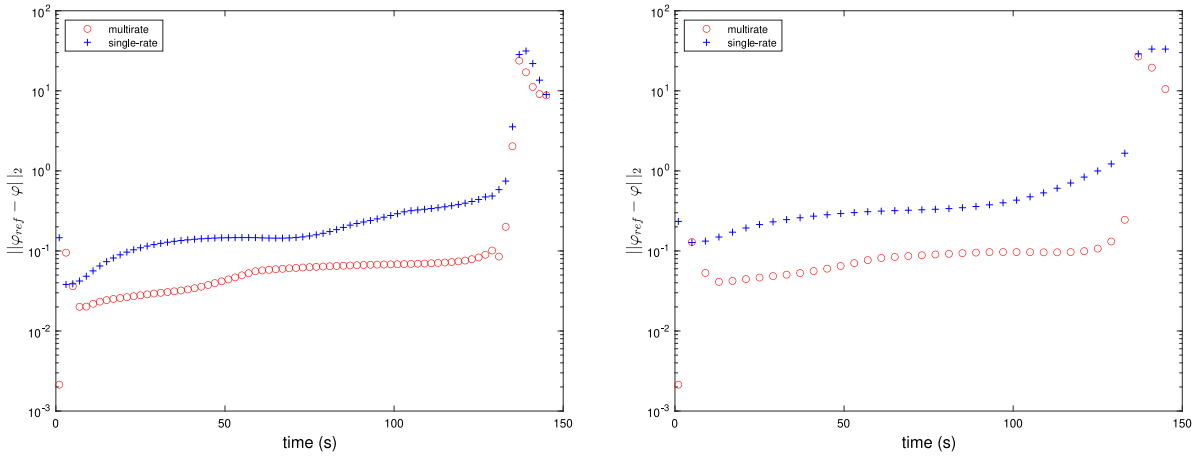

(a) q=2, $\Delta t = 4\Delta t_{ref}$ (b) q=4, $\Delta t = 4\Delta t_{ref}$

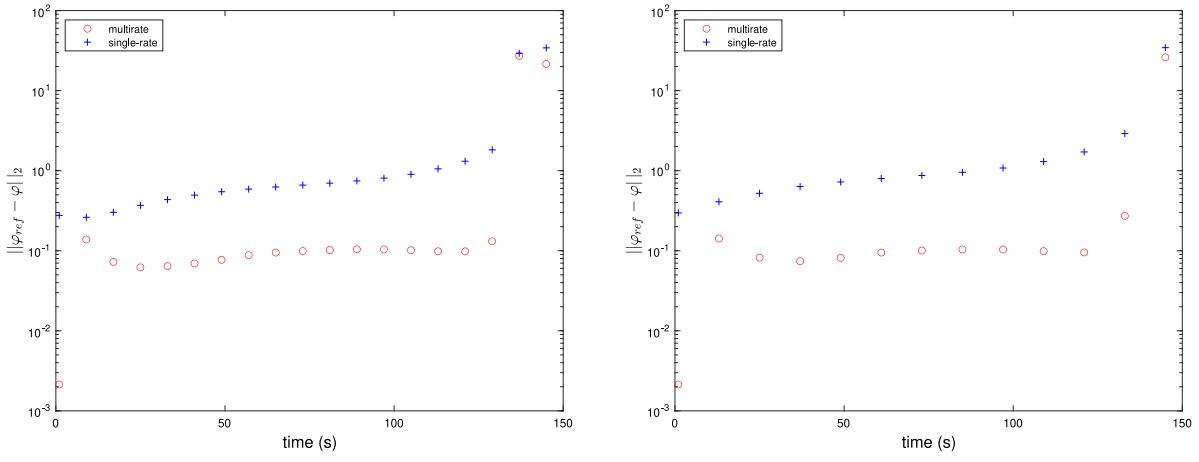

(c) q=8, $\Delta t = 8\Delta t_{ref}$ (d) q=12, $\Delta t = 12\Delta t_{ref}$

Fig. 12. Example 2: The error of different coarse time steps (Δt) is plotted over the simulation time for multirate and single-rate formulations.

As boundary conditions, we set the displacements to zero on $\partial\Omega$. The domain is discretized uniformly with 64 × 64 square elements with $h = 0.0625$ m.

4.2.2. Parameters

The fracture toughness is chosen as $G_c = 1.0N/m$. The mechanical parameters are Young's modulus and Poisson's ratio $E_s = 1.0Pa$ and $\nu_s = 0.2$. The relationship to the Lamé coefficients μ_s and λ_s is given by:

$$\mu_s = \frac{E_s}{2(1+\nu_s)}, \qquad \lambda_s = \frac{\nu_s E_s}{(1+\nu_s)(1-2\nu_s)}.$$

The regularization parameters are chosen as $\varepsilon = 2h$ and $\kappa = 10^{-10}h$. The penalization parameter is chosen as $\gamma = 10^3$ and the Lagrange multiplier is set to $\Xi^0 = 0$. Furthermore, the tolerance for the augmented Lagrangian iteration is $TOL = 10^{-4}$.

4.2.3. Updating the pressure function

At each time step the pressure load p is increased. Using the extrapolated scheme we prescribe:

$$p(t) = 0.16 + t \cdot \bar{p}, \qquad 0s \leq t \leq 144s,$$

where $\bar{p} = 0.001$ and t denotes the current time.

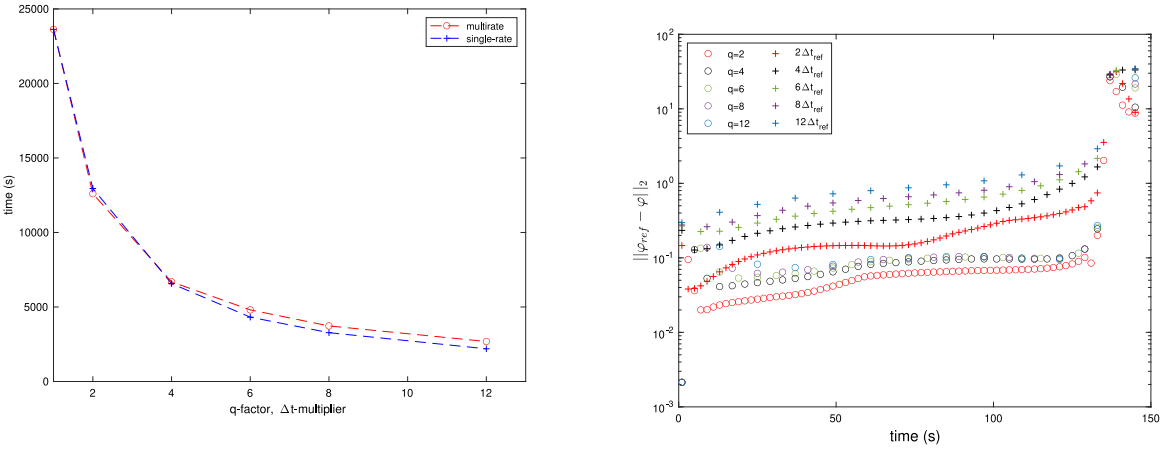

(a) Total simulation time for the single-rate and multirate schemes. Points are connected for visualization preferences.

(b) Error in phase-field variable over time

Fig. 13. Example 2: Comparison of speedup and accuracy of the multirate scheme. On the left, the total simulation time for the multirate scheme is compared to the single-rate formulation with a coarse time step. On the right, a comparison of the error in the phase-field solution for different q-factors is shown.

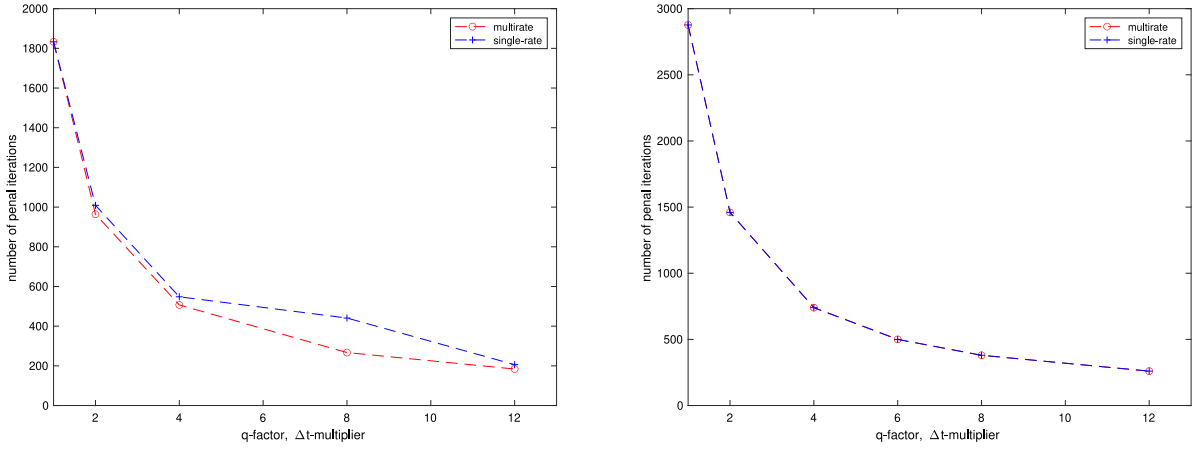

Fig. 14. Total number of penalization iterations (indexed by i in Algorithm 2) accumulated over all time steps n for different values of q. At left Example 1 and at right Example 2.

4.2.4. Results

In the reference test case, we use a fine time step ($\Delta t_{ref} = 1$ s) to track the fracture growth as the pressure increases (Fig. 9). Numerical simulations were conducted for this example by taking five different coarse time steps: $\Delta t = 2$ s, $\Delta t = 4$ s, $\Delta t = 6$ s, $\Delta t = 8$ s, and $\Delta t = 12$ s with the corresponding q-factors: 2, 4, 6, 8, and 12 for the multirate simulations.

The fracture paths at the end of propagation for the single-rate and multi-rate schemes are presented in Fig. 10 and Fig. 11, respectively. The results clearly show that using a coarse time step with a single-rate scheme failed to trace the fracture path of the reference test case (Fig. 10 b, c, and d). The multirate formulation captures the fracture propagation even for the case with $\Delta t = 12\Delta t_{ref}$.

The error of using the multirate scheme is consistently lower than that of the single-rate scheme over all time steps (Fig. 12). The computational cost of the additional iterations of the multirate scheme is relatively small; the total simulation time of the single-rate and multirate schemes are comparable (Fig. 12a). In fact, for $q = 2$, the multirate scheme in this example is slightly faster than the single-rate due to the faster convergence of the augmented-Lagrangian iteration.

The computational cost and error in the phase-field variable are shown in Fig. 13. The total number of penalization steps (iteration index i) accumulated over all time steps n for both numerical tests are provided in Fig. 14. Therein, the number of iterations is displayed for different choices of q.

4.3. Discussion

In the two presented examples, the multirate scheme significantly increased the accuracy of the phase-field solution over the simulation time; at some instances the increase was by more than 2-orders of magnitude. More evidently, in the pressurized fracture propagation example, the multirate scheme enabled tracking the fracture propagation with a coarse time step, which was not feasible with the single-rate scheme.

The multirate scheme allows using a larger choice of time step (Δt), without sacrificing the stability of computing the phase-field variable (φ). The error of calculating displacements $\mathbf{u}$ with a coarser time step will affect the accuracy of the phase-field solution φ. For this reason, using very large multirate factors (e.g. $q = 12$ in examples 1 and 2) might not be suitable for all classes of problems.

In general, the algorithm works well for problems that include fast fracture propagation with slower changes in displacements. It enables retaining the computational efficiency of using a coarse time step with an increased accuracy and stability. As usual, the choice of the of time step and multirate factor combination that is going to work best is problem-dependent and can be determined via numerical testing.

5. Conclusions

In this work, we proposed a multirate scheme for decoupling the mechanics equation and the phase-field equation for modeling fracture propagation. We provided algorithmic developments and studied the performance for two numerical examples. The first example was a pure mechanics test. The second example contains the extension to pressurized fracture in which the pressure is given. This constitutes the mechanics step in fractured porous media. An ongoing development is the extension to treat fluid-filled fractures in the pressure-step [31]. The final goal is to include these algorithmic developments into our phase-field fracture porous media software package Integrated Phase-Field Advanced Crack Propagation Simulator (IPACS) [12].

CRediT authorship contribution statement

Mohamad Jammoul: Contributions in Section 3, modifying the programming code, running the numerical examples, discussion on the numerical examples. **Mary F. Wheeler:** Contributions in the introduction, discussions in Section 3 and Section 4, and the conclusions, supervision of author 1. **Thomas Wick:** Contributions in the introduction, Section 2, partially in Section 3, Discussion of the numerical examples in Section 4 and also providing the first version of the programming code, Contributions in the conclusions.

Acknowledgments

We thank both anonymous referees for their numerous remarks and questions, which helped to improve significantly the first version of the manuscript. The work of M. Jammoul is supported by the Center for Subsurface Modeling (CSM), USA affiliates program. M.F. Wheeler is supported by the CSM, USA affiliates program and the National Science Foundation (NSF), USA grant *High-fidelity modeling of poromechanics with strong discontinuities* with the number 1911320. T. Wick is supported by the German Research Foundation, Priority Program 1748 (DFG SPP 1748) named *Reliable Simulation Techniques in Solid Mechanics. Development of Non-standard Discretization Methods, Mechanical and Mathematical Analysis* in the sub-project (WI 4367/2-1) under the project number 392587580. Moreover, T. Wick thanks the Center for Subsurface Modeling at the Oden Institute, UT Austin, for support during the stay in November 2019.

References

[1] R. Elliott, C.M. Matthews, As shale wells age, gap between forecasts and performance grows, Wall Street J. (2019).
[2] G. Francfort, J.-J. Marigo, Revisiting brittle fracture as an energy minimization problem, J. Mech. Phys. Solids 46 (8) (1998) 1319–1342.
[3] A. Griffith, The phenomena of rupture and flow in solids, Philos. Trans. R. Soc. Lond. 221 (1921) 163–198.
[4] B. Bourdin, G. Francfort, J.-J. Marigo, Numerical experiments in revisited brittle fracture, J. Mech. Phys. Solids 48 (4) (2000) 797–826.
[5] C. Miehe, F. Welschinger, M. Hofacker, Thermodynamically consistent phase-field models of fracture: variational principles and multi-field FE implementations, Int. J. Numer. Methods Eng. 83 (2010) 1273–1311.
[6] M. Jammoul, B. Ganis, M. Wheeler, General semi-structured discretization for flow and geomechanics on diffusive fracture networks, in: SPE Reservoir Simulation Conference, Society of Petroleum Engineers, 2019.
[7] M. Jammoul, B. Ganis, M.F. Wheeler, Effect of reservoir properties on interwell stress interference, in: 52nd US Rock Mechanics/Geomechanics Symposium, American Rock Mechanics Association, 2018.
[8] M. Jammoul, M.F. Wheeler, Modeling energized and foam fracturing using the phase field method, in: Unconventional Resources Technology Conference, 2020.
[9] A. Mikelić, M. Wheeler, T. Wick, A Phase-Field Approach to the Fluid Filled Fracture Surrounded by a Poroelastic Medium, ICES Report 13–15, 2013, Jun.
[10] A. Mikelić, M.F. Wheeler, T. Wick, A quasi-static phase-field approach to pressurized fractures, Nonlinearity 28 (5) (2015) 1371–1399.
[11] M. Wheeler, T. Wick, W. Wollner, An augmented-Lagangrian method for the phase-field approach for pressurized fractures, Comput. Methods Appl. Mech. Eng. 271 (2014) 69–85.

[12] M.F. Wheeler, T. Wick, S. Lee, IPACS: Integrated Phase-Field Advanced Crack Propagation Simulator. An adaptive, parallel, physics-based-discretization phase-field framework for fracture propagation in porous media, Comput. Methods Appl. Mech. Engrg. 367 (2020) 113124.
[13] T. Wick, Multiphysics Phase-Field Fracture: Modeling, Adaptive Discretizations, and Solvers, in: Radon Series on Computational and Applied Mathematics, de Gruyter, 2020, Band 28.
[14] M. Fortin, R. Glowinski, Augmented Lagrangian Methods: Applications to the Numerical Solution of Boundary Value Problems, in: Stud. Math. Appl., vol. 15, North Holland, Amsterdam, 1983.
[15] R. Glowinski, P.L. Tallec, Augmented Lagrangian and Operator-Splitting Methods in Nonlinear Mechanics, in: SIAM Stud. Appl. Math., vol. 9, SIAM, Philadelphia, 1989.
[16] K. Ito, K. Kunisch, Lagrange Multiplier Approach to Variational Problems and Applications, in: Advances in Design and Control, vol. 15, Society for Industrial and Applied Mathematics (SIAM), Philadelphia, PA, 2008.
[17] B. Bourdin, Numerical implementation of the variational formulation for quasi-static brittle fracture, Interfaces Free Bound. 9 (2007) 411–430.
[18] B. Bourdin, G. Francfort, J.-J. Marigo, The Variational approach to fracture, J. Elasticity 91 (1–3) (2008) 1–148.
[19] S. Burke, C. Ortner, E. Süli, An adaptive finite element approximation of a variational model of brittle fracture, SIAM J. Numer. Anal. 48 (3) (2010) 980–1012.
[20] A. Mesgarnejad, B. Bourdin, M. Khonsari, Validation simulations for the variational approach to fracture, Comput. Methods Appl. Mech. Engrg. 290 (2015) 420–437.
[21] F. List, F.A. Radu, A study on iterative methods for solving Richards' equation, Comput. Geosci. 20 (2) (2016) 341–353.
[22] I.S. Pop, F. Radu, P. Knabner, Mixed finite elements for the Richards' equation: linearization procedure, J. Comput. Appl. Math. 168 (1–2) (2004) 365–373.
[23] M.K. Brun, T. Wick, I. Berre, J.M. Nordbotten, F.A. Radu, An iterative staggered scheme for phase field brittle fracture propagation with stabilizing parameters, Comput. Methods Appl. Mech. Engrg. 361 (2020) 112752.
[24] T. Almani, K. Kumar, G. Singh, M. Wheeler, Stability of multirate explicit coupling of geomechanics with flow in a poroelastic medium, Comput. Math. Appl. 78 (8) (2019) 2682–2699.
[25] T.M. Almani, Efficient Algorithms for Flow Models Coupled with Geomechanics for Porous Media Applications (Ph.D. thesis), The University of Texas at Austin, 2016.
[26] I. Rybak, J. Magiera, R. Helmig, C. Rohde, Multirate time integration for coupled saturated/unsaturated porous medium and free flow systems, Comput. Geosci. 19 (2) (2015) 299–309.
[27] M.F. Wheeler, C.N. Dawson, An operator-splitting method for advection-diffusion-reaction problems, in: J.A. Whiteman (Ed.), MAFELAP Proceedings, Vol. VI, Academic Press, 1988, pp. 463–482.
[28] L. Ambrosio, V. Tortorelli, Approximation of functionals depending on jumps by elliptic functionals via Γ-convergence, Comm. Pure Appl. Math. 43 (1990) 999–1036.
[29] L. Ambrosio, V. Tortorelli, On the approximation of free discontinuity problems, Boll. Unione Mat. Ital. B 6 (1992) 105–123.
[30] A. Mikelić, M.F. Wheeler, T. Wick, Phase-field modeling through iterative splitting of hydraulic fractures in a poroelastic medium, GEM - Int. J. Geomath. 10 (1) (2019).
[31] A. Mikelić, M.F. Wheeler, T. Wick, A phase-field method for propagating fluid-filled fractures coupled to a surrounding porous medium, SIAM Multiscale Model. Simul. 13 (1) (2015) 367–398.
[32] S. Lee, M.F. Wheeler, T. Wick, Pressure and fluid-driven fracture propagation in porous media using an adaptive finite element phase field model, Comput. Methods Appl. Mech. Engrg. 305 (2016) 111–132.
[33] T. Wick, An error-oriented Newton/inexact augmented Lagrangian approach for fully monolithic phase-field fracture propagation, SIAM J. Sci. Comput. 39 (4) (2017) B589–B617.
[34] C. Miehe, M. Hofacker, F. Welschinger, A phase field model for rate-independent crack propagation: Robust algorithmic implementation based on operator splits, Comput. Methods Appl. Mech. Engrg. 199 (2010) 2765–2778.
[35] H. Amor, J.-J. Marigo, C. Maurini, Regularized formulation of the variational brittle fracture with unilateral contact: Numerical experiments, J. Mech. Phys. Solids 57 (2009) 1209–1229.
[36] M. Ambati, T. Gerasimov, L. De Lorenzis, A review on phase-field models of brittle fracture and a new fast hybrid formulation, Comput. Mech. 55 (2) (2015) 383–405.
[37] N. Kikuchi, J. Oden, Contact Problems in Elasticity, in: Studies in Applied Mathematics, Society for Industrial and Applied Mathematics (SIAM), Philadelphia, PA, 1988.
[38] K. Mang, T. Wick, W. Wollner, A phase-field model for fractures in nearly incompressible solids, Comput. Mech. 65 (2020) 61–78.
[39] P.G. Ciarlet, The Finite Element Method for Elliptic Problems, 2. pr. ed., North-Holland, Amsterdam [u.a.], 1987.
[40] C. Engwer, S.I. Pop, T. Wick, Dynamic and weighted stabilizations of the L-scheme applied to a phase-field model for fracture propagation, 2019, arXiv:1912.07096.
[41] T. Gerasimov, L.D. Lorenzis, A line search assisted monolithic approach for phase-field computing of brittle fracture, Comput. Methods Appl. Mech. Engrg. (2015).
[42] T. Wick, Modified Newton methods for solving fully monolithic phase-field quasi-static brittle fracture propagation, Comput. Methods Appl. Mech. Engrg. 325 (2017) 577–611.
[43] T. Davis, I.S. Duff, An unsymmetric-pattern multifrontal method for sparse LU factorization, SIAM J. Matrix Anal. Appl. 18 (1) (1997) 140–158.
[44] T. Bittencourt, P. Wawrzynek, A. Ingraffea, J. Sousa, Quasi-automatic simulation of crack propagation for 2D LEFM problems, Eng. Fract. Mech. 55 (2) (1996) 321–334.